P3.10 ACCOUNTING FOR MULTIPLE SCATTERING IN SPACEBORNE RADAR AND LIDAR OBSERVATIONS

ROBIN J. HOGAN[1]* AND ALESSANDRO BATTAGLIA[2]

[1]*Department of Meteorology, University of Reading, United Kingdom*
[2]*Meteorological Institute, University of Bonn, Germany*

ABSTRACT

CloudSat observations of deep convective clouds reveal significant contributions from multiply scattered photons, resulting in "pulse stretching", where echoes appear to originate from beyond the end of the cloud and even below the ground. Spaceborne lidar returns from liquid water clouds suffer from the same effect. It is essential to account for this phenomenon if we are to retrieve accurate microphysical profiles from space, but no satisfactory method for doing so has yet been devised. In this paper an efficient multiple scattering model is described that may be incorporated into retrieval schemes as the "forward model" for both radar and lidar, thereby allowing multiple scattering to be accounted for. It splits the photons into those that have taken a near-direct path out to and back from a single backscattering event (in the case of lidar, accounting for small-angle forward scatterings on the way), and those that have experienced wide-angle multiple-scattering events leading to pulse stretching. The latter are modeled using the time-dependent two-stream approximation, which reduces the problem to solving a pair of coupled partial differential equation. The method performs well in comparison to Monte Carlo calculations, but is far more efficient. This offers the prospect not only of accounting for a troublesome effect in CloudSat and Calipso data, but also of making use of multiple scattering to extract extra information about clouds and convective systems.

1. Introduction

Lidar and radar have been used extensively from the ground to study clouds (Illingworth et al. 2007) but from space (Stephens et al. 2002; Winker et al. 2003) the interpretation of the backscattered signals is made more complicated by the much larger instrument footprints, which result in a greater fraction of the detected photons having undergone multiple scattering. It was shown by Hogan et al. (2006) that if consideration of lidar multiple-scattering effects are omitted in combined radar-lidar retrievals of ice clouds from space then the retrieved optical depth will be underestimated by around 40%. Hogan (2006) introduced a fast lidar forward model for the case when the multiple scattering is dominated by quasi-small-angle forward scattering events, as is usually the case for ground-based lidar observations. Delanoë and Hogan (2007) have recently implemented this into a variational retrieval scheme.

In this paper we consider the more general case when wide-angle multiple scattering becomes important. The particular difficulty to contend with in this regime is that the associated time delay makes returning photons appear to have originated from a range beyond the distance to which they actually penetrated, an effect known as "pulse stretching". This is particularly evident for spaceborne cloud radar and lidar due to the large detector footprint on the cloud: for lidar this occurs in observations of liquid water clouds (Platt and Winker 1995), and for 94-GHz radar in deep convective clouds (Battaglia et al. 2007a).

There is potentially useful information available on the properties of cloud that can, in principle, be extracted from measurements subject to wide-angle multiple scattering. For example, the technique of "off-beam lidar" utilizes a single laser transmitter but a receiver array with a range of fields-of-view (Davis et al. 1999). The different degrees of multiple scattering to which each field-of-view is sensitive allows the optical depth of liquid clouds to be estimated. Furthermore, lidar backscattering from water droplets retains the transmitted polarization, resulting in very low measured lidar depolarization ratio, but in the presence of wide-angle multiple scattering, the measured returns become progressively more depolarized with further penetration into the cloud.

The most rigorous method for interpreting measurements from active sensors is using a variational approach, in which a first guess of the profile of atmospheric properties is successively refined based on its ability to "forward model" the measurements. The difficulty with treating wide-angle multiple scattering is that until now there has been no forward model that is fast enough to use in a retrieval scheme. Monte-Carlo methods have been used to model both lidar (Platt 1981) and radar (Battaglia and Mantovani 2005) multiple-scattering. Obviously these are not fast enough to use in a retrieval scheme directly, but Cahalan et al. (2005) performed off-line Monte-Carlo simulations on a finite set of idealized cloud profiles, then constructed a retrieval that essentially searched for the simulation that best matched the observations. While this approach benefits from the accuracy of the Monte-Carlo calculations, the library of off-line calculations clearly cannot represent all possible combinations of variables.

Other theoretical work used so far to interpret wide-angle multiple scattering has been based on diffusion theory (Davis et al. 1999), which is appropriate for very

* *Corresponding author address:* Department of Meteorology, Earley Gate, PO Box 243, Reading RG6 6BB, United Kingdom. E-mail: r.j.hogan@reading.ac.uk.

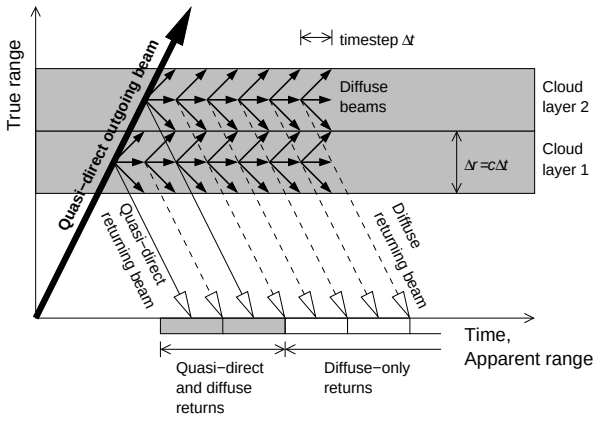

FIG. 1: Schematic "space-time" diagram illustrating the essentials of the algorithm. The thick arrow depicts the propagation of a transmitted beam towards a two-layer cloud. Some of the radiation is backscattered towards the receiver (solid open-headed arrows), and its travel time (distance on the abscissa) may be interpreted directly in terms of range to the cloud. Some is scattered into diffuse streams inside the cloud, with the possibility of being subsequently scattered back toward the receiver (dashed open-headed arrows). In this case the travel time cannot be interpreted directly as a depth of penetration into the cloud.

optically thick media where photons rapidly lose memory of their initial direction, but is not suited for more mixed profiles where photons have a ballistic behaviour in optically thinner regions and a diffusive behaviour in optically thicker regions. It is also not suitable for use on its own, since the returns from the first few optical depths into even an optically thick cloud are dominated by single scattering and quasi-small-angle scattering. More recently, Kobayashi et al. (2006) and Ito et al. (2007) have developed an analytical model that includes pulse stretching, but only second-order scattering is included, and the method is not fast enough to use in retrieval algorithms (Battaglia et al. 2007b).

In this paper a method is described that is accurate and efficient enough to use as a forward model in retrieval schemes both for radar and lidar multiple scattering. In section 2 an overview of the method is presented and the time-dependent two-stream stream approximation introduced. In section 3, the contribution to apparent backscatter from those photons that have *not* experienced wide-angle scattering is calculated. Then in section 4, the numerical integration of the time-dependent two-stream equations for calculating the wide-angle component is described. Comparison with Monte Carlo calculations is provided in 5.

2. Overview of method

The method is best described by reference to the "space-time" diagram in Fig. 1. The solid line indicates the outgoing "quasi-direct" beam, containing unscattered photons propagating away from the instrument at speed c and, in the case of lidar, photons that have undergone small-angle forward scattering but are still considered to be part of the same beam. The cloud and aerosol profile is discretized into layers of thickness Δr, which are assumed to be homogeneous in the directions perpendicular to the quasi-direct beam. It is also assumed that the pulse length is less than or equal to Δr. The very small fraction of photons in the quasi-direct beam that are backscattered towards the receiver can return to the instrument along quasi-direct path (i.e. allowing for small-angle forward scattering on the return journey). They arrive at a time t (on the horizontal axis in Fig. 1) that may be unambiguously converted into the apparent range r using $r = 2ct$. Section 3 describes this part of the calculation, which uses the algorithm developed by Hogan (2006).

The photons in the quasi-direct beam that experience wide-angle scattering within the cloud then enter the diffuse distribution, which is modeled at each range gate by an outgoing and an incoming stream $I^{\pm}$ travelling in two discrete directions. Their evolution is governed by the time-dependent two-stream (TDTS) equations:

$$\frac{1}{c}\frac{\partial I^+}{\partial t} = -\mu_1 \frac{\partial I^+}{\partial r} - \mu_1 \alpha \left(\gamma_1 I^+ - \gamma_2 I^-\right) + S^+, \quad (1)$$

$$\frac{1}{c}\frac{\partial I^-}{\partial t} = -\mu_1 \frac{\partial I^-}{\partial r} - \mu_1 \alpha \left(\gamma_1 I^- - \gamma_2 I^+\right) + S^-, \quad (2)$$

where the coefficients γ_1 and γ_2 are given by

$$\gamma_1 = \left[1 - \tilde{\omega}(1+g)/2\right]/\mu_1, \quad (3)$$

$$\gamma_2 = \tilde{\omega}(1-g)/(2\mu_1), \quad (4)$$

and the medium is described by the standard range-dependent quantities extinction coefficient α, single-scattering albedo $\tilde{\omega}$ and asymmetry factor g. The cosine of the angle between these streams and the outgoing direction is $\pm\mu_1$, such that these streams propagate away from the instrument at a speed $\pm\mu_1 c$. The two streams are represented in Fig. 1 by the short 45° arrows (note that the short horizontal arrows simply represent the fraction of the diffuse radiation that does not leave a particular layer within the timestep Δt).

It can be seen that (1) and (2) are simply the standard time-*independent* two-stream equations but with the addition of a time derivative on the left-hand side. The time-independent form is used in the radiation schemes of almost all weather forecast and climate models (Meador and Weaver 1980; Zdunkowski et al. 1982; Edwards and Slingo 1996; Stephens et al. 2001; Shonk and Hogan 2007), where the equations are solved as a boundary value problem. In modeling the propagation of a short pulse of radiation we simply add the time-derivative terms to yield a pair of coupled partial differential equations, which are solved as an initial value problem. To the authors' knowledge, the only previous use of the time-dependent two-stream equations was by Ayoubi and Nelson (1989), who tackled the lidar multiple scattering problem but only in the quasi-small-angle limit.

The terms on the right-hand side of (1) and (2) each have a straighforward interpretation. The first represents radiative transport from one range-gate to another and is exactly analogous to the advection term in the Navier-Stokes equations of fluid dynamics. The second term represents loss of energy from a stream by scattering

and absorption (governed by γ_1) and the gain of energy by scattering from the other stream (governed by γ_2). The final terms $S^{\pm}$ are functions of both r and t, and represent the source of energy from the quasi-direct beam. Note that the calculation of the source terms is exactly analogous to a short-wave time-independent two-stream radiation scheme, in which the direct solar beam is used to calculate the source terms used by the two-stream equations to estimate the diffuse radiative fluxes as a function of height. In the present case the lidar or radar sources perform the same role as the sun. Section 3 describes how the source terms are calculated, while section 4 describes how (1) and (2) are numerically integrated forward in time.

Although the method is applicable to both lidar and radar, the conventional unit for expressing the measured range-normalized intensity is different. For simplicity we use the usual lidar variable "apparent backscatter" $\hat{\beta}$ (in $\mathrm{m}^{-1}\ \mathrm{sr}^{-1}$) throughout the paper, defined as the backscatter coefficient of the medium that a measured intensity would correspond to in the absense of attenuation or multiple scattering. At radar wavelengths the radar backscatter coefficient may be converted to "apparent radar reflectivity factor" by the following (Donovan et al. 2001)

$$\hat{Z} = \frac{4}{|K_l|^2}\left(\frac{\lambda}{\pi}\right)^4 \hat{\beta}, \tag{5}$$

where $|K_l|^2$ is a reference "dielectric factor" of liquid water. Some calibration conventions use the value at centimeter wavelengths, 0.93, while others use the value at the frequency in question, but it should be noted that at millimeter wavelengths it is temperature dependent. See Hogan et al. (2003) for further discussion of radar calibration conventions.

3. Calculation of the quasi-direct component and the source terms for the diffuse calculation

a. Radar: single scattering

For radar observations of clouds and precipitation, where the diameter of the largest particles is, at most, of the same order as the wavelength, the quasi-direct component of the apparent backscatter, $\hat{\beta}_d$ is described simply by

$$\hat{\beta}_d(r) = \beta(r)\exp\left[-2\delta(r)\right], \tag{6}$$

where β is the true backscatter coefficient of the medium and $\delta(r) = \int_0^r \alpha\,\mathrm{d}r$ is the optical depth of the medium to range r. As explained by Hogan (2006), if range gate i represents ranges from r to $r+\Delta r$ (over which the backscatter coefficient β_i and extinction coefficient α_i are constant) then the apparent backscatter averaged across the gate is

$$\hat{\beta}_{d,i} = \beta_i \exp\left[-2\delta(r_i)\right]\frac{1-\exp(-2\alpha_i\Delta r)}{2\alpha_i\Delta r}. \tag{7}$$

The next step is to calculate the source terms for the diffuse calculation. The diffuse radiances in each direction, $I_{i,j}^{\pm}$, are normalized such that they represent the fraction of the initial transmitted energy that is present in a particular gate i in a particular timestep j in a particular direction. Therefore, the source terms S_i^+ and S_i^- represent the fraction of the total transmitted energy that enters the outgoing and incoming diffuse beams, respectively, at range gate i at time r_i/c after the pulse is transmitted. First, the average transmission to gate i, τ_i, is calculated, which is simply the one-way equivalent of the transmission part of (7):

$$\tau_i = \exp\left[-\delta(r_i)\right]\left[1-\exp(-\alpha_i\Delta r)\right](\alpha_i\Delta r)^{-1} \tag{8}$$

The fraction of the initial energy scattered into the diffuse distribution at gate i is therefore $\tilde{\omega}_i\alpha_i\tau_i$, where $\tilde{\omega}$ is the single-scattering albedo of the medium. To determine what fraction enters the outgoing stream and what fraction enters the incoming stream, we make use of the two-stream phase function (e.g. Fu et al. 1997). In the case of scattering from the outgoing beam ($\mu = 1$) into the two streams ($\mu = \pm\mu_1$) this predicts $P(1,\pm\mu_1) = (1\pm 3g\mu_1)/2$, where g is the asymmetry factor of the medium. Note that the phase function has been normalized such that the integral of P over a sphere is unity. Thus the source terms at gate i are given by

$$S_i^{\pm} = \tilde{\omega}_i\alpha_i\tau_i\left(1\pm 3g_i\mu_1\right)/2. \tag{9}$$

For $g > 2/3$, this equation results in the unphysical $S^- < 0$, so instead in this instance we use $S_i^+ = \tilde{\omega}_i\alpha_i\tau_i$ and $S_i^- = 0$.

The final step is to calculate the spatial variance of the photons in the unscattered beam when they reach gate i, needed in section 4b. If the transmitted photon distribution from the instrument may be described as a Gaussian with a $1/e$ angular half-width of ρ_{tr}, then the variance of the spatial photon distribution at range r is simply

$$\overline{s^2}_d = \rho_{\mathrm{tr}}^2 r^2. \tag{10}$$

b. Lidar: quasi-small-angle multiple scattering

When the characteristic size of the scatterers is much larger than the wavelength of the radiation, as is the case in most lidar cloud remote sensing, half of the photons that interact with a scatterer will be diffracted around the particle, forming a narrow "foward scattering lobe" in the phase function. The remaining half intecept the particle and are then either scattered into a wide distribution of angles (forming the large-angle component of the phase function), or absorbed. We treat the forward-scattered photons as being part of the "quasi-direct beam", behaving almost if they had not been scattered at all.

In order to determine the apparent backscatter due to the quasi-direct beam, $\hat{\beta}_d$, we use the "Photon Variance-Covariance" (PVC) model described by Hogan (2006). By calculating the variance and covariance of photon position and direction as a function of range, it achieves O(N^2) efficiency for an N-point profile and includes photons that have been forward scattered an arbitrary number of times on the outgoing or return journeys.

To describe what happens to the widely scattered photons, it is appropriate to define what will be referred

to as "diffraction-scaled" values for the extinction coefficient, single-scattering albedo and asymmetry factor:

$$\alpha'' = \alpha/2, \quad (11)$$

$$\tilde{\omega}'' = 2\tilde{\omega} - 1, \quad (12)$$

$$g'' = g + (g-1)/\tilde{\omega}''. \quad (13)$$

This transformation is analogous to "delta-M" scaling (Joseph et al. 1976) used in section 4, but is more appropriate here when we only wish to remove the narrow forward lobe that has already been dealt with by the Hogan (2006) model, not the often larger fraction of the forward phase function that is removed by delta-M scaling. It should be noted that in deriving (12) we have assumed that, as in Mie theory, an absorbing particle only absorbs photons that are directly intercepted by it, not those that are diffracted into the forward lobe. Therefore the minimum value of $\tilde{\omega}$ represented by this approach is 0.5 (for which $\tilde{\omega}'' = 0$).

At each range gate, these values are combined with the corresponding unscaled values for molecular scattering and absorption, and then used to calculate a scaled optical depth $\delta(r)$ for use in calculating the transmission and source terms using (8) and (9). It should be noted that both delta-M scaled and diffraction-scaled values have been tried in the algorithm, but only diffraction scaling provided satisfactory agreement with Monte Carlo calculations.

For lidar, the calculation of the spatial variance of the photons in the quasi-direct beam, $\overline{s^2}_d$, needs to include not only the unscattered photons described by (10), but also the broadening effect caused by the contribution from the forward-scattered photons.

4. Calculation of the diffuse component

This section describes the contribution to the backscatter from the photons that have experienced wide-angle multiple scattering. First, in section 4a, the TDTS equations are used to estimate the diffuse radiances in each direction as a function of time and range from the instrument. Since the photons spread out laterally, we need to calculate what fraction of this energy remains within the instrument field-of-view. This is achieved in section 4b by modeling the spatial variance of photon position using essentially the same equations. Finally in section 4c, the reciever pattern is used to estimate the intensity of the returned radiation as a function of time.

a. Integration of the time-dependent two-stream equations

Equations (1) and (2) are integrated on a discrete grid in time and space, where for convenience, the timestep Δt is related to the grid spacing Δr (assumed to be regular) by $\Delta t = \Delta r/c$. This ensures that in one timestep the quasi-direct beam will travel a distance Δr, while in the optically thin limit the diffuse streams will travel $\pm\mu_1\Delta r$. Several different values for μ_1 have been proposed in the literature (Meador and Weaver 1980), but in this application, the best *a posteriori* agreement with Monte-Carlo calculations is found for $\mu_1 = 1/2$.

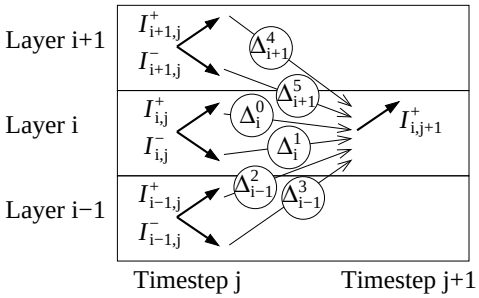

FIG. 2: Schematic illustrating how coefficients Δ^0 to Δ^5 in (15) control how the outgoing radiance $I^+_{i,j+1}$ at timestep $j+1$ is determined by the radiances in adjacent layers at timestep j.

For lidar observing particles much larger than the wavelength, the standard delta-M scaling (Joseph et al. 1976) is used to account for the narrow forward lobe in the phase function, and all further use of these variables in the context of lidar refers to the delta-M-scaled versions. For radar, the particles are at most of a similar scale to the wavelength of the radiation, so no delta-M scaling is applied.

In order to solve (1) and (2), we first consider the case for $\mu_1\alpha\gamma_2 c\Delta t \ll 1$, which corresponds to the limit when the probability of a photon being scattered into the other direction within a single timestep is much less than unity. In this limit we can discretize (1) using an explicit forward timestep and the spatial derivative using a simple upstream scheme. So if $I^+_{i,j}$ represents the outgoing radiance at range-gate i and timestep j, then the radiance at the subsequent timestep is given by

$$I^+_{i,j+1} = I^+_{i,j} + c\Delta t\left[\mu_1\left(I^+_{i-1,j} - I^+_{i,j}\right)/\Delta r - \mu_1\alpha\left(\gamma_1 I^+_{i,j} - \gamma_2 I^-_{i,j}\right) + S^+_{i,j}\right], \quad (14)$$

and similarly for $I^-_{i,j+1}$. The radiances are initialized to zero, and hence the energy enters the system purely through the source terms $S^\pm_{i,j}$. Because the timestep is such that the direct beam travels exactly one range gate in one timestep, $S^\pm_{i,j}$ is only non-zero when $i = j$.

When $\mu_1\alpha\gamma_2 c\Delta t$ exceeds unity, the simple discretization of (14) cannot be used because it predicts that more radiaton is transfered to the other stream than is actually present, leading to numerical instability. The problem is that many scattering events may occur within a single timestep, so the system represented by the coupled partial differential equations (1) and (2) has become "stiff". A solution is to define 6 coefficients at each range gate, Δ^0_i to Δ^5_i, expressing what fraction of the energy in $I^+_{i,j}$ is transfered into adjacent range gates (or remains at the same range gate in the case of Δ^0_i) in a single timestep. In this way the forward step is implemented by

$$I^+_{i,j+1} = \Delta^0_i I^+_{i,j} + \Delta^1_i I^-_{i,j} + \Delta^2_{i-1} I^+_{i-1,j} + \Delta^3_{i+1} I^-_{i+1,j} + \Delta^4_{i+1} I^+_{i+1,j} + \Delta^5_{i-1} I^-_{i-1,j} + c\Delta t S^+_{i,j}, \quad (15)$$

and similarly for $I^-_{i+1,j}$. This is illustrated in Fig. 2. The coefficients are defined once for a given profile, and include the possibility of multiple scattering within a sin-

gle timestep. The calculation of these coefficients is described in the Appendix.

b. The variance of the photon distribution

To describe the rapid lateral spreading of the photon distribution with time, we need to model the spatial variances of the photon distribution, $\overline{s^2}_w^{\pm}$ (with the subscript w denoting photons arising from wide-angle scattering to distinguish from $\overline{s^2}_d$). In the case that diffusion theory is applicable, the evolution of the spatial variance would be expected to be governed by

$$\partial \overline{s^2}_w / \partial t = D, \tag{16}$$

where D is the diffusivity of the medium. To account for the transport of photon variance from one gate and one stream to another, we consider the energy-weighted variances $J^+ = I^+ \overline{s^2}_w^+$ and $J^- = I^- \overline{s^2}_w^-$. The evolution of these quantities may be described in exactly the same way as the diffuse radiances, as follows:

$$\frac{1}{c}\frac{\partial J^+}{\partial t} = -\mu_1 \frac{\partial J^+}{\partial r} - \mu_1 \alpha \left(\gamma_1 J^+ - \gamma_2 J^-\right) + S^+ \overline{s^2}_d + D I^+, \tag{17}$$

$$\frac{1}{c}\frac{\partial J^-}{\partial t} = -\mu_1 \frac{\partial J^-}{\partial r} - \mu_1 \alpha \left(\gamma_1 J^- - \gamma_2 J^+\right) + S^- \overline{s^2}_d + D I^-. \tag{18}$$

These are essentially the same as (1) and (2), except that the source term from the quasi-direct beam also includes its variance $\overline{s^2}_d$, and an additional source term appears due to the horizontal diffusion of photons with effective diffusivity D.

In terms of discretization, (17) and (18) may be treated in exactly the same way as (1) and (2), using an equation analogous to (15) with the same coefficients. When required, the variances may be recovered by dividing through by the diffuse radiances: $\overline{s^2}_w^{\pm} = J^{\pm}/I^{\pm}$.

The key to accurate calculation of the spatial variance is clearly in the appropriate specification of the diffusivity. When diffusion theory is applicable, the diffusivity is given by (Davis and Marshak 2001)

$$D = \frac{4}{3} c l_t, \tag{19}$$

where l_t is the transport mean free path:

$$l_t = [\alpha(1 - \tilde{\omega} g)]^{-1}. \tag{20}$$

Note that the coefficient $4/3$ is appropriate when we are considering diffusion in a three-dimensional medium but only considering the variance of position in the two dimensions lateral to the instrument axis. Unfortunately, diffusion theory is not applicable until a number of scattering events have taken place; if (19) is substituted directly into (16) then it can be shown that the initial evolution of the variance implies faster-than-light travel, which is clearly unphysical.

To investigate how $\overline{s^2}_w$ evolves, simple Monte Carlo calculations have been carried out in which a distribution of photons is initialised within an infinite, homogeneous cloud of isotropic scatterers, and the photon trajectories modeled over time. The initial distribution is assumed to be Gaussian in the x and y directions (centered at $x = y = 0$) and a delta function in the r direction (at $r = 0$), with a random initial direction. This approximately represents photons that have been scattered from the quasi-direct beam into the diffuse distribution, as described in section 3. Figure 3 shows the evolution of the spatial variance $\overline{s^2}_w = \overline{x^2} + \overline{y^2}$ with time, with both axes normalized to make the results applicable to a medium with any value of l_t. An excellent fit to the Monte Carlo calculations is given by

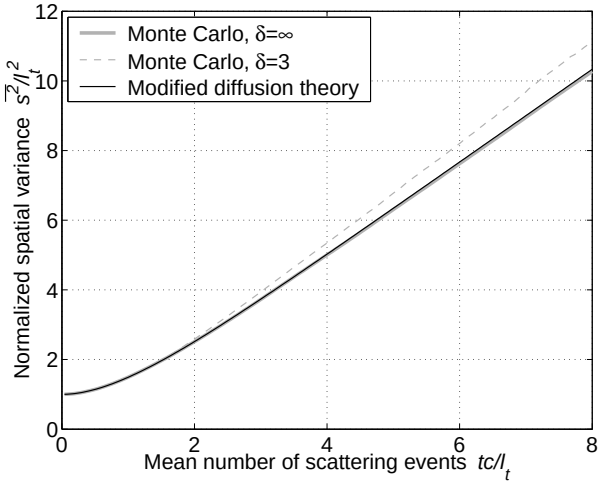

FIG. 3: Monte Carlo calculation of the evolution of the variance of photon position in the x and y directions from an initial value of $\overline{s^2}_w = l_t^2$ (where l_t is the transport mean-free-path) at time $t = 0$. Scattering is isotropic and is plotted against the mean number of scattering events $\bar{n} = tc/l_t$. The thick gray line corresponds to Monte Carlo calculations in an infinite domain, whereas the thin dashed gray line considers a cloud that is finite in the r direction (orthogonal to x and y) with an optical depth $\delta = 3$. The photons are initialised in the centre of the cloud in the r direction, and those that escape are not considered in the calculation of the spatial variance. The solid black line shows the analytic formula given by (21). The Monte Carlo calculations used 2×10^4 photons.

$$\overline{s^2}_w = \overline{s^2}_d + \frac{4}{3} l_t^2 \left(\bar{n} + e^{-\bar{n}} - 1\right), \tag{21}$$

where $\overline{s^2}_d$ is the spatial variance at the initial time $t = 0$, and the mean number of scattering events is $\bar{n} = tc/l_t$. It is easy to show that in the limit of many scattering events ($\bar{n} \gg 1$), the time derivative of $\overline{s^2}_w$ follows diffusion theory as described by (16) and (19), while in the limit of few scattering events ($\bar{n} \ll 1$), we have $\partial(\overline{s^2}_w)^{1/2}/\partial t \simeq (2/3)^{1/2} c$. This latter case corresponds to a spherical shell of unscattered photons expanding out at the speed of light from their point of origin.

In order to implement this behavior alongside transport in the r direction, an alternative formulation for D in (17) and (18) is required. We first need to estimate $\bar{n}$ from each of $\overline{s^2}_w^+$ and $\overline{s^2}_w^-$. Unfortunately, (21) cannot be inverted directly, so instead we make a first guess of $\bar{n}$ by

inverting one of the two asymptotic forms for $\bar{n}$, depending on the value of $(\overline{s^2}_w - \overline{s^2}_d)/l_t^2$:

$$\begin{array}{ll} (\overline{s^2}_w - \overline{s^2}_d)/l_t^2 = (2/3)\bar{n}^2; & (\overline{s^2}_w - \overline{s^2}_d)/l_t^2 < 0.8, \\ (\overline{s^2}_w - \overline{s^2}_d)/l_t^2 = (4/3)(\bar{n}-1); & (\overline{s^2}_w - \overline{s^2}_d)/l_t^2 \geq 0.8. \end{array} \tag{22}$$

One step of Newton's method in log-log space is sufficient to obtain an accurate value at timestep j, $\bar{n}_j$. At the next timestep, the mean number of scattering events will be $\bar{n}_{j+1} = \bar{n}_j + c\Delta t/l_t$. We can therefore use (21) to obtain the effective diffusivity:

$$D = \frac{\overline{s^2}_{w,j+1} - \overline{s^2}_{w,j}}{\Delta t} = \frac{4l_t^2}{3\Delta t}\left(\bar{n}_{j+1} - \bar{n}_j + e^{-\bar{n}_{j+1}} - e^{-\bar{n}_j}\right). \tag{23}$$

This is applied in (17) and (18) at each range gate and each timestep. It is assumed that exactly the same formulation is applicable for non-isotropic scattering, although in this case $\bar{n}$ would be the *effective* mean number of scattering events. An alternative approach would be to adapt the approximate relationships given by Platnick (2001).

As a final point, it should be noted that despite the good fit to the Monte Carlo results in Fig. 3, other factors can limit the accuracy of (21). In particular, in an optically thin cloud, the photons that escape from the top or bottom of the cloud will preferentially be those with a smaller lateral variance, with the result that those photons that remain in the cloud will tend to have a higher lateral variance than would be expected in an infinite cloud. To illustrate this, the dashed line in Fig. 3 shows a Monte Carlo calculation for a cloud with an optical depth of $\delta = 3$ and it can be seen that as the number of scattering events increases, (21) increasingly underestimates the lateral variance. However, as δ increases, the behavior quickly approaches that for $\delta = \infty$. One way to represent this could be to multiply the first term on the right-hand-side of (17) and (18) by a factor between 0 and 1, thereby representing the fact that the photons that are transported in the direction r tend to be those that have a lower variance in the x and y directions. However, theory would have to be developed to parameterize such a factor in terms of variables available to the TDTS method.

c. Calculation of apparent backscatter

The final step is to calculate the apparent backscatter due to wide-angle scattering, $\hat{\beta}$, by considering the fraction of photons at each range gate and time step that are scattered directly back towards the reciever and detected. This involves convolving the photon distribution with the receiver pattern and accounting for losses on the return journey. The apparent backscatter component due to scattering from the diffuse photon distribution at range gate i at time step j, travelling away from $(+)$ and towards $(-)$ the receiver, is given by

$$\Delta\hat{\beta}_{i,j}^{\pm} = \frac{\tilde{\omega}_i\alpha_i\tau_i(1 \mp 3g_i\mu_1)}{4\pi} \times \frac{\int_0^\infty E_{i,j}^{\pm}(s)R_i(s)s\,\mathrm{d}s}{\int_0^\infty T_i(s)R_i(s)s\,\mathrm{d}s}, \tag{24}$$

where the first term on the right hand side represents the probability that photons are scattered towards the receiver and accounts for the transmission on the return journey. It can be derived in an analogous way to the source term given by (9), but note that in the case of lidar we here use the usual delta-M-scaled values, rather than the "diffusion scaled" values. The factor of 4π ensures that the apparent backscatter has the units of $\mathrm{m}^{-1}\,\mathrm{sr}^{-1}$. The second term on the right consists of a convolution of the photon distribution $E^{\pm}(s)$ with the reciever pattern $R(s)$, where s is the lateral distance from the reciever axis. This is normalized by a convolution of the transmitter pattern $T(s)$ with the reciever pattern.

We assume that the transmitter pattern and the lateral photon distributions can be described by Gaussians as follows:

$$T_i(s) = \frac{1}{\pi\rho_{\mathrm{tr}}^2 r_i^2}\exp\left(-\frac{s^2}{\rho_{\mathrm{tr}}^2 r_i^2}\right), \tag{25}$$

$$E_i^{\pm}(s) = \frac{I^{\pm}}{\pi\overline{s^2}_w^{\pm}}\exp\left(-\frac{s^2}{\overline{s^2}_w^{\pm}}\right). \tag{26}$$

Note that the transmitter pattern is normalized so that its integral over all s is unity, i.e. $2\pi\int_0^\infty T_i(s)s\,\mathrm{d}s = 1$.

The reciever pattern may be described by either a Gaussian (appropriate for a radar antenna) or a top-hat function (appropriate for a lidar telescope). In the former case, when the same antenna is used for transmission and receiption, the receiver pattern is the same, i.e. $R_i = T_i$. Substitution of these functions into (24) yields

$$\Delta\hat{\beta}_{i,j}^{\pm} = \frac{\tilde{\omega}_i\alpha_i\tau_i(1 \mp 3g_i\mu_1)}{4\pi} \times \frac{2I_i^{\pm}}{1 + \overline{s^2}_{w,i}^{\pm}/\left(\rho_{\mathrm{tr}}r_i\right)^2}. \tag{27}$$

In the case of a lidar, the reciever pattern may be represented by

$$R_i(s) = \begin{cases} 1/\pi\rho_{\mathrm{fov}}^2; & s \leq \rho_{\mathrm{fov}} \\ 0; & s > \rho_{\mathrm{fov}} \end{cases}, \tag{28}$$

which results in

$$\Delta\hat{\beta}_{i,j}^{\pm} = \frac{\tilde{\omega}_i\alpha_i\tau_i(1 \mp 3g_i\mu_1)}{4\pi} \times I_i^{\pm}\frac{1 - \exp\left(-\rho_{\mathrm{fov}}^2 r_i^2/\overline{s^2}_{w,i}^{\pm}\right)}{1 - \exp\left(\rho_{\mathrm{fov}}^2/\rho_{\mathrm{tr}}^2\right)}. \tag{29}$$

The wide-angle apparent backscatter is calculated by summing up the appropriate values of $\Delta\hat{\beta}_{i,j}$. The complication is that while apparent backscatter is output on the same grid as the input variables (α_i, $\tilde{\omega}_i$ and g_i), the time step j must be taken into account as it leads to returns appearing to originate further from the instrument. This is best explained with reference to Fig. 1: to work out the returned power a particular "apparent" range on the abscissa, we must sum up the contributions from each range gate and timestep the diagonal path of the returning beams. The result is that a given combination of range gate i and timestep j will appear to have originated from a range $r = r_i + (j-i)c\Delta t/2$. In terms of measured backscatter at apparent range gate k, we have the following summation:

$$\hat{\beta}_{w,k} = \sum_{n=0}^{k}\Delta\hat{\beta}_{n,2k-n}^{+} + \Delta\hat{\beta}_{n,2k-n+1}^{+} + \Delta\hat{\beta}_{n,2k-n}^{-} + \Delta\hat{\beta}_{n,2k-n+1}^{-}. \tag{30}$$

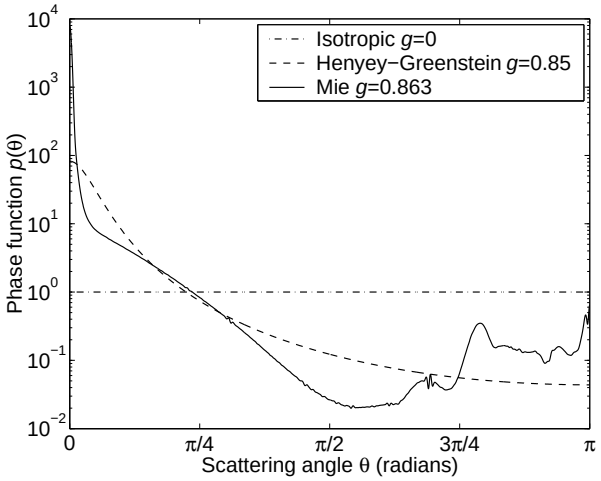

FIG. 4: Three scattering phase functions used to test the multiple scattering model in the lidar configuration. The Mie calculation is performed for liquid droplets with an effective radius of 10 μm. The phase function is defined such that its integral over all directions is equal to the scattering efficiency, which is equal to 2 for non-absorbing scatterers in the geometric optics limit.

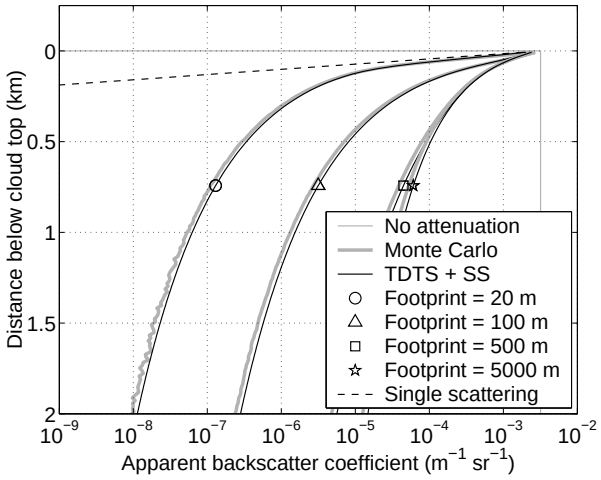

FIG. 5: Comparison of apparent backscatter for I3RC Experiment 1, which consists of a semi-infinite cloud of non-absorbing isotropic scatterers, as described in the section 5a. The thick gray lines show the calculations of the Monte Carlo model of Battaglia and Mantovani (2005), while the solid black lines show the results for the new method, in this case using a combination of time-dependent two-stream (TDTS) method and single scattering (SS).

Finally, this wide-angle apparent backscatter must be added to the quasi-direct backscatter from (7) to obtain the total apparent backscatter.

5. Comparison against Monte Carlo calculations

In this section the fast multiple scattering model developed in this paper will be compared to the Monte Carlo model of (Battaglia and Mantovani 2005), for both lidar and radar cases.

a. Spaceborne lidar

Three of the cases from the Intercomparison of 3D Radiation Codes (I3RC) are used to demonstrate the ability of the model to represent different kinds of phase function, as shown in Fig. 4. The first case (I3RC Experiment 1) considers a semi-infinite horizontally homogeneous cloud with an extinction coefficient of 0.04 m^{-1} that is illuminated by an instantaneous pulse of photons with zero lateral width in a direction normal to the plane of the cloud. The scatterers are assumed to be isotropic and non-absorbing.

To model the backscatter measured from this cloud, we use a combination of single scattering and wide-angle scattering modeled by the TDTS method. A range-gate spacing of 15 m is used, and the receiver is assumed to have a top-hat response function. Figure 5 shows the apparent backscatter as a function of apparent range below cloud top for four receiver fields-of-view, corresponding to footprints between 20 m and 5000 m.

Good agreement can be seen between the Monte Carlo and the TDTS for all instrument fields-of-view, even at apparent distances well below the cloud where all of the returned signal is due to wide-angle multiple scattering. In common with all the lidar comparisons in this section, the TDTS model appears to overestimate the backscatter to a modest degree. This is believed to be due to the fact that cloud is illuminated by a point beam of photons, the initial lateral distribution of which is rather poorly described by a Gaussian. This is likely to be less of a problem for real spaceborne lidars for which laser source provides photons with a distribution of finite width that may be reasonably described by a Gaussian.

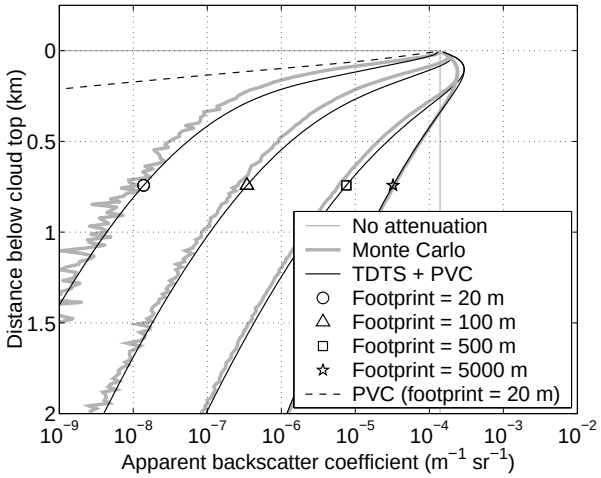

FIG. 6: As Fig. 6, but for the second case described in section 5a (I3RC Experiment 3). This consists of a semi-infinite cloud of absorbing particles with a single scattering albedo of $\tilde{\omega} = 0.98$ and the Henyey-Greenstein phase function shown in Fig. 4.

The second case (I3RC Experiment 3) considers the same semi-infinite cloud as in the first case, but with a single-scattering albedo of $\tilde{\omega} = 0.98$ and a Henyey-

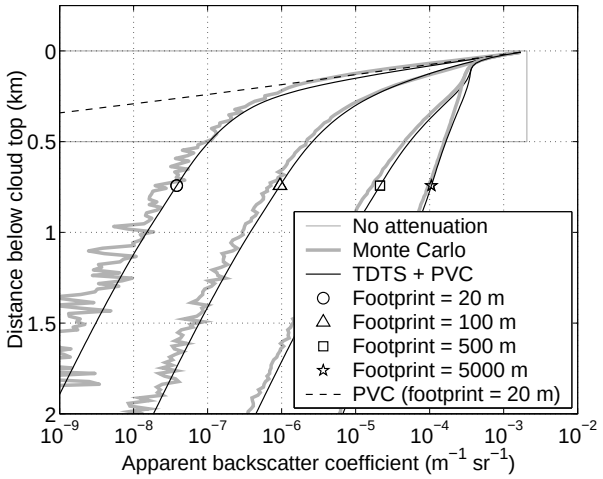

FIG. 7: As Fig. 5 but for the third case described in section 5a (I3RC Experiment 5) in which the cloud is 500-m thick, has an optical depth of 20, and the scattering is described by the Mie phase function shown in Fig. 4.

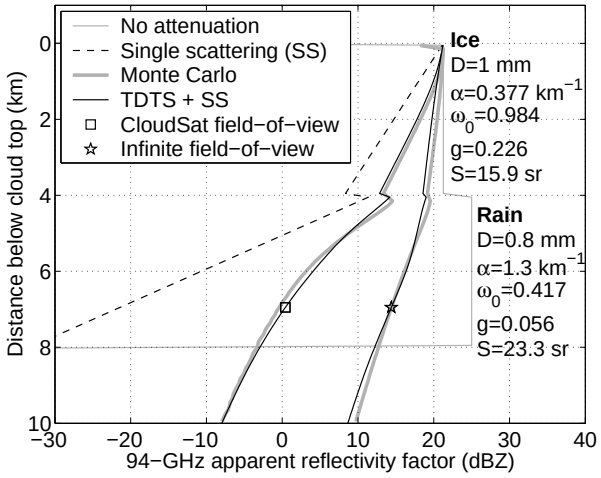

FIG. 8: Comparison of apparent radar reflectivity factor for the case described section 5b.

Greenstein phase function with $g = 0.85$, as illustrated by the dashed line in Fig. 4. The cloud is illuminated by a point source of photons as before. This case is modeled by a combination of quasi-small-angle multiple scattering using the Photon Variance-Covariance (PVC) method described by Hogan (2006) and the TDTS method. The PVC method describes the forward lobe as a Gaussian with a the $1/e$ half-width of $\Theta = 0.138$ radians, and assumes an isotropic phase function in the near-backscatter direction. Delta-M scaling is used. The results are shown in Fig. 6.

The backscatter profile within the cloud is rather different than in Fig. 5. This is because the backscatter coefficient (i.e. the value of the phase function at $\theta = \pi$ in Fig. 4) is much less. This leads to a considerably smaller fraction of the returned photons originating from single scattering and quasi-small-angle multiple scattering (the component that is calculated using the PVC method); rather the wide-angle multiple scattering is dominant (the component calculated using the TDTS method). The performance of the TDTS method is somewhat worse than in Fig. 5, probably due to the fact that the Henyey-Greenstein phase function contains an unrealistically wide forward lobe that blends smoothly into rest of the phase function, so there is a less obvious transition between quasi-small-angle scattering and wide-angle scattering. Note that the noise in the Monte Carlo calculations is due to the finite number of photons used.

The third case (I3RC Experiment 5) considers a non-absorbing 500-m cloud of optical depth 20 with a phase function described by Mie theory, for a lognormal droplet-size distribution with an effective radius of 10 μm and a standard deviation that is 0.3 times the mean radius. The "equivalent-area radius" (required by the PVC method) for such a distribution is $r_a = 11.96$ μm. This is again modeled by by a combination of the PVC and TDTS methods, and the results are shown in Fig. 7.

The agreement within the cloud is much better than for the Henyey-Greenstein phase function. This is presumably because there is a clear transition between quasi-small-angle forward scattering (caused by the sharp forward lobe a few degrees from $\theta = 0$ in Fig. 4) and wide-angle scattering. The backscatter profile in the top-most 50-m of the cloud is very different than in Fig. 6 due to the peak in the phase function in the backscatter direction, which enhances the quasi-small-angle multiple scattering return relative to the wide-angle return.

b. Spaceborne radar

To evaluate the performance of the new multiple scattering model for spaceborne 94-GHz radar, we use an idealized profile based on Scenario 3 of Battaglia et al. (2007b). This consists of a 4-km layer of 1-mm ice spheres overlying a 4-km layer of 0.8-mm raindrops, with the properties indicated to the right of Fig. 8 (note that S is the extinction-to-backscatter ratio). The total optical depth of the cloud is 6.7. The pulse length is 100 m and the radiation is assumed to be unpolarized. The radar is at an altitude of 715 km and is assumed to have a Gaussian transmitter pattern with a $1/e$ half-angle beam divergence of $\rho_{\rm tr} = 1.13$ mrad, similar to CloudSat. The reference dielectric factor in (5) is $|K_l|^2 = 0.75$.

Figure 8 compares the Monte Carlo model and the new model (using the sum of the TDTS and single scattering returns) for a receiver with the same Gaussian pattern as the transmitter (the "CloudSat field-of-view") and an infinite field-of-view. Very good agreement is again observed. It should be noted that this is a rather less challenging case than the lidar comparisons in the previous section: firstly, for particles smaller than the wavelength, the phase function has a very simple shape (not shown). Secondly, the transmitter and receiver have the same Gaussian response patterns, which means that the assumption that the lateral photon distribution is also described by a Gaussian is adequate.

Figures 9 and 10 compare the total energy and root-

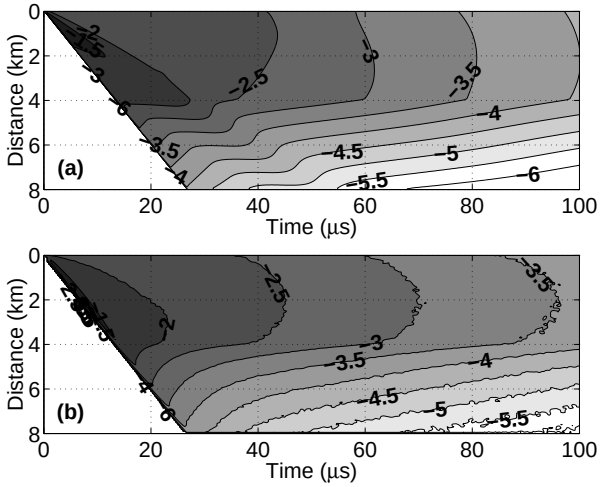

FIG. 9: The base-10 logarithm of the total diffuse radiative energy in a given level as a function of time and distance below cloud top for the radar case shown in Fig. 8, calculated by (a) the TDTS model, and (b) the Monte Carlo model. So in the case of the TDTS model, the quantity shown is $\log_{10}(I^+ + I^-)$.

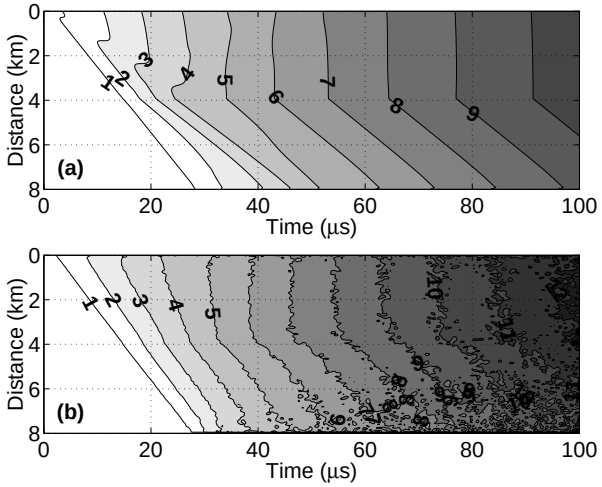

FIG. 10: As Fig. 9 but for the root-mean-squared horizontal deviation of photons from the radar axis, in kilometers. In the case of the TDTS model (panel a), the quantity shown is $\sqrt{(J^+ + J^-)/(I^+ + I^-)}$.

mean-squared horizontal displacement of the photons within the cloud as a function of time and distance below cloud top. The diagonal edge to the left of each panel corresponds to the incoming direct beam. Reasonable agreement is evident for both variables, although as time progresses there is a slight tendency for the TDTS model to underestimate both of them. There is evidence for weak artefacts introduced by the two-stream approximation: both Figs. 9a and 10a exhibit kinks in the contours corresponding to a broad ray propagating out from the origin with a speed of $c/2$. However, this does not appear to have fed through significantly to the backscatter in Fig. 8.

6. Conclusions

A fast model has been described to calculate the time-dependent multiple scattering returns from radar and lidar. It uses a hybrid approach, with the quasi-small-angle multiple-scattering returns characteristic of lidar being calculated by the Photon Variance-Covariance (PVC) method of Hogan (2006), and the wide-angle multiple scattering that occurs for both radar and lidar being calculated using the Time-Dependent Two-Stream (TDTS) approximation described here. Both components of the model are O(N^2) efficient for an N-point profile, and on a 1-GHz Pentium 3 the execution time for $N = 50$ for the PVC component it is 0.6 ms, while for the TDTS component it is 2.5 ms (the Monte Carlo calculations for the equivalent profile take several hours to execute). This makes it particularly suitable for use as the "forward model" in spaceborne retrieval schemes (e.g. (Delanoë and Hogan 2007)), where a new profile is recorded approximately every 100 ms. It is also useful when taking the approach of evaluating the representation of clouds in climate and forecast models by forward-modeling the observed variables, something that has recently been done for the IceSAT lidar and the ECMWF model (Wilkinson et al. 2007).

A number of developments of the TDTS model are planned. Firstly, there is a need to find a fast method to estimate the Jacobian matrix, i.e. the derivative of the attenuated backscatter with respect to each of the input variables, in particular the extinction coefficient at each range gate. This is required if the model is to be used as part of a variational retrieval scheme (Rodgers 2000). A common feature of spaceborne lidar and radar observations is of multiply scattered cloud echoes appearing to originate from beneath the ground. In order to forward-model this phenomenon, it is necessary to include the surface reflection in the model. This capability has recently been added to the Battaglia and Mantovani (2005) Monte Carlo code, which will be used to test its implementation in the TDTS code. Finally, a further piece of information available when multiple scattering occurs is from the depolarization ratio, since in a medium that normally does not depolarize (e.g. liquid water droplets observed by lidar), the effect of multiple scattering is to progressively depolarize the light such that, in principle, this variable provides information on the number of scatteirng events that have occurred. In order to interpret such measurements correctly, the capability to model the depolarization due to multiple scattering will be added to both the PVC and TDTS models.

Appendix: Discretizing the 2-stream equations in optically thick media

As discussed at the end of section 4a, for optically thick media (specifically those with $l_t \lesssim \Delta r$) a simple discretization of the time-dependent two-stream equations such as (14) is inaccurate and may be numerically unstable. A solution is to use the discretization given in (15), in which the coefficients Δ_i^0 to Δ_i^5 are precomputed at each gate i. These coefficients describe how an initial radiance $I_{i,j}^+$ (or $I_{i,j}^-$) at timestep j is distributed amongst the outgo-

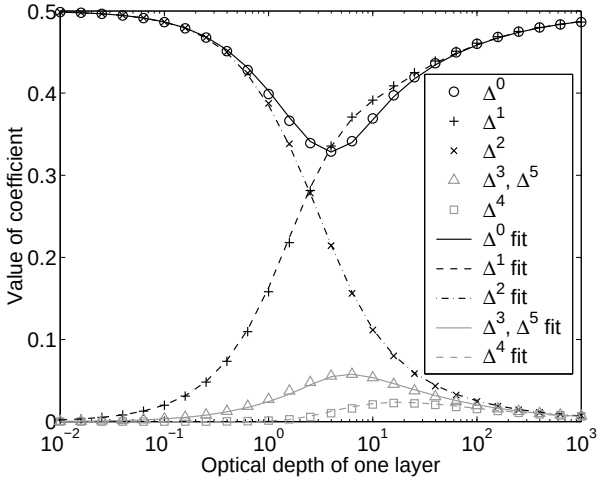

FIG. 11: Values of the coefficients introduced in (15), versus the optical depth of a single model level, for a cloud with $\tilde{\omega} = 1$ and $g = 0.45$. The symbols are derived from a high resolution run of the time-dependent two-stream equations (as described in the Appendix), while the lines represent semi-empirical fits to these points as described by (31)-(39). Note that this value of g corresponds to $g = 0.82$ after delta-M scaling.

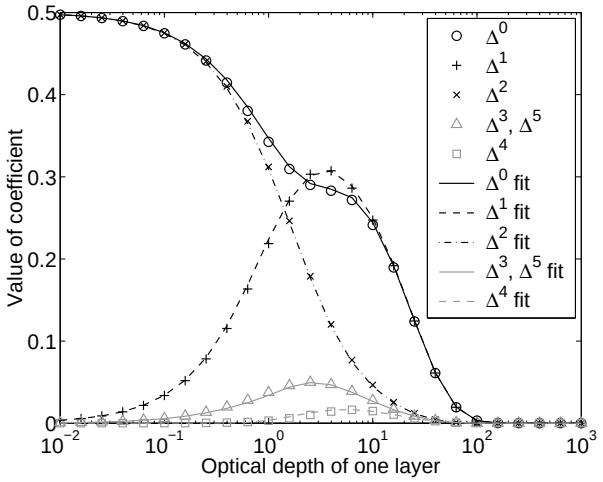

FIG. 12: As Fig. 11 but for $\tilde{\omega} = 0.95$ and $g = 0$.

ing and incoming radiances in the adjacent range gates at the subsequent timestep $j+1$. This appendix outlines how these coefficients are derived.

For simplicity, we assume that the properties of range gates $i+1$ and $i-1$ are the same as at gate i; this ensures that the Δ_i coefficients only depend on the properties at gate i. The photons that constitute the radiance $I^+_{i,j}$ are assumed to be travelling in the same direction $+\mu_1$. In a single timestep $\Delta t = \Delta r/c$, the total distance travelled by an unabsorbed photon will be Δr. However, we are interested in the mean distance travelled in the direction towards or away from the instrument in a single timestep. In the two-stream approximation, the maximum that this can be is $\mu_1 \Delta r$.

Our approach is semi-empirical. First, high-resolution runs of the time-dependent two-stream method are performed to estimate the coefficients as a function of the optical depth within a single range gate, using the simple discretization of (14). In each simulation, a one-dimensional grid between $r = -\Delta r$ and $r = 2\Delta r$ is initialized with $I^+ = 1$ between $r = 0$ and $r = \Delta r$ and $I^+ = 0$ elsewhere, while I^- is set to 0 everywhere. The high-resolution grid spacing $\Delta r'$ is chosen to ensure that the optical depth within a single high-resolution layer is less than 0.05. The simulation is run for time $\Delta t = \Delta r/c$, but using timesteps of $\Delta t' = \Delta r'/c$. At the end of the simulation, the six coefficients are calculated as the fraction of the initial energy that has been transported to each of the two directions and three ranges of Δr in the domain. The results for $\tilde{\omega} = 1$ and $g = 0.45$ are shown by the symbols in Fig. 11, as a function of the optical depth of one layer. Figure 12 shows the same but for an absorbing layer.

The next step is to fit these computations analytically. When one attempts to calculate analytically the distance that radiation will be transported in the scenario described above, it becomes clear that four particular variables must be important. These four variables are now derived. They are then combined to fit the modeled points indicated in Figs. 11 and 12, and heuristic arguments are presented to explain the analytical expressions.

The first variable is the fraction of photons that will remain unscattered after a single timestep:

$$F_t = \exp\left(-\Delta r/l_t\right), \tag{31}$$

where l_t is the transport mean-free-path (see Eq. 20). The second variable is the fraction of photons that are unabsorbed (although they may be scattered) after a single timestep:

$$F_a = \exp\left(-\Delta r/l_a\right), \tag{32}$$

where $l_a = [\alpha(1-\tilde{\omega})]^{-1}$ is the absorption mean-free-path. Of those photons that are scattered before a timestep has elapsed, the mean fraction of a range gate that has been travelled at the point of scattering provides our third variable, given by

$$\begin{aligned} L &= \frac{1}{\Delta r}\int_0^{\Delta r} \mu_1 r \exp(-r/l_t)\mathrm{d}r \Big/ \int_0^{\Delta r} \exp(-r/l_t)\mathrm{d}r \\ &= \mu_1\left[\frac{l_t}{\Delta r} - \frac{F_t}{(1-F_t)}\right]. \end{aligned} \tag{33}$$

Last, we consider the behaviour in the optically thick limit, when there are many scattering events within the timestep. In this situation, diffusion theory may be applied, and the fraction of the radiaition that diffuses from one layer to the next in a single timestep provides the fourth variable:

$$L_d = \mu_1 F_a (l_t/3\Delta r)^{1/2}. \tag{34}$$

Expressions for the coefficients are derived by assuming that the total transport from one gate and direction to another can be described by the sum of a non-diffusive component, which dominates in the optically thin limit and

involves the first three variables, and a diffusive component, which dominates in the optically thick limit and involves the fourth variable. The non-diffusive transport component essentially describes the transport of photons that have some memory of their initial direction within a single timestep.

A combination of empirical fitting and physical insight was used to derive the following fits to the points in Figs. 11 and 12:

$$\begin{aligned}
\Delta^0 &= F_t(1-\mu_1) + (F_a - F_t)(1/2 - L) \\
&\quad - L_d C_0, \qquad (35)\\
\Delta^1 &= (F_a - F_t)(1-L)/2 - L_d C_1, \qquad (36)\\
\Delta^2 &= \mu_1 F_t + (F_a - F_t)L + L_d C_0/2, \qquad (37)\\
\Delta^3 &= \Delta^5 = (F_a - F_t)L/4 + L_d C_1/2, \qquad (38)\\
\Delta^4 &= L_d C_0/2, \qquad (39)
\end{aligned}$$

where the empirical terms scaling the diffusive transport are

$$\begin{aligned}
C_0 &= \exp\left[-3.7(l_t/\Delta r)^{3/4}\right], \qquad (40)\\
C_1 &= \exp\left[-3.7(l_t/\Delta r)\right]. \qquad (41)
\end{aligned}$$

These two terms simply correct for the fact that at low optical depths ($l_t \ll \Delta r$), diffusion theory (expressed by L_d) predicts excessively high transport.

The non-diffusive transport terms (those involving F_a, F_t and L) may be understood physically. For example, consider Δ^2, which describes the transport from one gate to the next in the same direction. The first term on the right-hand-side of (37) expresses the fact that in one timestep, a fraction F_t of the photons are not scattered or absorbed, so travel a fraction μ_1 of a range gate. The second term states that an additional fraction $F_a - F_t$ of the photons are scattered after travelling a fraction L of a range gate, on average. Similar arguments may be used to understand the other non-diffusive transport terms.

Acknowledgements. We thank Tamás Várnai for coordinating the I3RC intercomparisons and providing the Mie phase function shown in Fig. 4.

REFERENCES

Ayoubi, I. S., and P. Nelson, 1989: Concentration profiles from lidar measurements in the presence of multiple scattering: the two-stream approximation. *Appl. Opt.,* **28,** 4133–4140.

Battaglia, A., and S. Mantovani, 2005: Forward Monte Carlo computations of fully polarized microwave radiation in non isotropic media. *J. Quant. Spectroscopy Rad. Transfer,* **95,** 285–308.

Battaglia, A., M. O. Ajewole and C. Simmer, 2007a: Evaluation of radar multiple scattering effects in CloudSat configuration. *Atmos. Chem. Phys.,* in press.

Battaglia, A., S. Kobayashi, S. Tanelli, C. Simmer and E. Im, 2007b: Multiple scattering effects in pulsed radar systems: an intercomparison study. *Submitted to J. Atmos. Oceanic Technol*.

Cahalan, R. F., M. McGill, J. Kolasinski, T. Várnai and K. Yetzer, 2005: THOR—Cloud thickness from offbeam lidar returns. *J. Atmos. Oceanic Technol.,* **22,** 605–627.

Davis, A. B., R. F. Cahalan, J. D. Spinhirne, M. J. McGill and S. P. Love, 1999: Off-beam lidar: An emerging technique in cloud remote sensing based on radiative Green-function theory in the diffusion domain. *Phys. Chem. Earth (B),* **24,** 757–765.

Davis, A. B., and A. Marshak, 2001: Multiple scattering in clouds: insights from three-dimensional diffusion/P_1 theory. *Nuclear Sci. Eng.,* **137,** 251–280.

Delanoë, J., and R. J. Hogan, 2007: A variational method for retrieving ice cloud properties from combined radar, lidar and infrared radiometer. *To be submitted to J. Appl. Meteorol*.

Donovan, D. P., A. C. A. P. van Lammeren, H. W. J. Russchenberg, A. Apituley, R. J. Hogan, P. N. Francis, J. Testud, J. Pelon, M. Quante and J. W. F. Goddard, 2001: Cloud effective particle size and water content profile retrievals using combined lidar and radar observations - 2. Comparison with IR radiometer and in situ measurements of ice clouds. *J. Geophys. Res.,* **106,** 27 449–27 464.

Edwards, J. M., and A. Slingo, 1996: Studies with a flexible new radiation code - 1. Choosing a configuration for a large scale model. *Quart. J. Roy. Meteorol. Soc.,* **122,** 689–719.

Fu, Q., K. N. Liou, M. C. Cribb, T. P. Charlock and A. Grossman, 1997: Multiple scattering parameterization in thermal infrared radiative transfer. *J. Atmos. Sci.,* **54,** 2799–2812.

Hogan, R. J., 2006: Fast approximate calculation of multiply scattered lidar returns. *Appl. Optics,* **45,** 5984–5992.

Hogan, R. J., D. P. Donovan, C. Tinel, M. A. Brooks, A. J. Illingworth and J. P. V. Poiares Baptista, 2006: Independent evaluation of the ability of spaceborne radar and lidar to retrieve the microphysical and radiative properties of ice clouds. *J. Atmos. Oceanic Technol.,* **23,** 211–227.

Hogan, R. J., D. Bouniol, D. N. Ladd, E. J. O'Connor and A. J. Illingworth, 2003: Absolute calibration of 94/95-GHz radars using rain. *J. Atmos. Oceanic Technol.,* **20,** 572–580.

Illingworth, A. J., R. J. Hogan, E. J. O'Connor, D. Bouniol, M. E. Brooks, J. Delanoë, D. P. Donovan, J. D. Eastment, N. Gaussiat, J. W. F. Goddard, M. Haeffelin, H. Klein Baltink, O. A. Krasnov, J. Pelon, J.-M. Piriou, A. Protat, H. W. J. Russchenberg, A. Seifert, A. M. Tompkins, G.-J. van Zadelhoff, F. Vinit, U. Willén, D. R. Wilson and C. L. Wrench, 2007: Cloudnet – Continuous evaluation of cloud profiles in seven operational models using ground-based observations. *Bull. Am. Meteorol. Soc.,* in press.

Ito, S., S. Kobayashi and T. Oguchi, 2007: Multiple scattering formulation of pulsed beam waves in hydrom-

eteors and its application to millimeter wave weather radar. *IEEE Geosci. Remote Sens. Lett.,* **4,** 13–17.

Joseph, J. H., W. J. Wiscombe and J. A. Weinman, 1976: The delta-Eddington approximation for radiative flux transfer. *J. Atmos. Sci.,* **33,** 2452–2459.

Kobayashi, S., T. Oguchi, S. Tanelli and E. Im, 2006: Backscattering enhancement on spheriod-shaped hydrometeors: considerations in water and ice particles of uniform size, and Marshall-Palmer distributed rains. *Radio Sci.,* **42,** doi:2006RS003503.

Meador, W. E., and W. R. Weaver, 1980: Two-stream approximations to radiative transfer in planetary atmospheres: a unified description of existing methods and a new improvement. *J. Atmos. Sci.,* **37,** 630–643.

Platnick, S., 2001: Approximations for horizontal photon transport in cloud remote sensing problems. *J. Quant. Spectoscopy Radiative Trans.,* **68,** 75–99.

Platt, C. M. R., 1981: Remote soundings of high clouds. 3 - Monte Carlo calculations of multiple-scattered lidar returns. *J. Atmos. Sci.,* **38,** 156–167.

Platt, C. M. R., and D. M. Winker, 1995: Multiple scattering effects in clouds observed from LITE. In *Optics in Atmospheric Propagation and Adaptive Systems,* Anton Kohnle, Ed. *Proc. SPIE,* **2580,** 60–71.

Rodgers, C. D., 2000: *Inverse methods for atmospheric sounding: Theory and practice.* World Scientific, pp. 238.

Shonk, J. K. P., and R. J. Hogan, 2007: Tripleclouds: an efficient method for representing cloud inhomogeneity in 1D radiation schemes by using three regions at each height. *Submitted to J. Climate*.

Stephens, G. L., P. M. Gabriel and P. T. Partain, 2001: Parameterization of atmospheric radiative transfer - 1. Validity of simple models. *J. Atmos. Sci.,* **58,** 3391–3409.

Stephens, G. L., D. G. Vane, R. J. Boain, G. G. Mace, K. Sassen, Z. Wang, A. J. Illingworth, E. J. O'Connor, W. B. Rossow, S. L. Durden, S. D. Miller, R. T. Austin, A. Benedetti, C. Mitrescu and the CloudSat Science Team, 2002: The CloudSat Mission and the A-Train. *Bull. Am. Meteorol. Soc.,* **83,** 1771–1790.

Wilkinson, J. M., R. J. Hogan, A. J. Illingworth and A. Benedetti, 2007: Use of a lidar forward model for global comparisons of cloud fraction between the ICESat lidar and the ECMWF model. *To be submitted to Mon. Weath. Rev*.

Winker, D. M., J. Pelon and M. P. McCormick, 2003: The CALIPSO mission: Spaceborne lidar for observation of aerosols and clouds. *Proc. SPIE,* **4893,** 1–11.

Zdunkowski, W. G., W.-G. Panhans, R. M. Welch and G. J. Korb, 1982: A radiation scheme for circulation and climate models. *Beitr. Phys. Atmos.,* **55,** 215–238.